



JAEA-Research

2024-011

DOI:10.11484/jaea-research-2024-011

Momentum Exchange Functions Model for SIMMER-III and SIMMER-IV

Yoshiharu TOBITA, Satoru KONDO and Tohru SUZUKI

Fast Reactor Cycle System Research and Development Center
Oarai Research and Development Institute

October 2024

Japan Atomic Energy Agency

日本原子力研究開発機構

JAEA-Research

本レポートは国立研究開発法人日本原子力研究開発機構が不定期に発行する成果報告書です。
本レポートの転載等の著作権利用は許可が必要です。本レポートの入手並びに成果の利用(データを含む)
は、下記までお問い合わせ下さい。

なお、本レポートの全文は日本原子力研究開発機構ウェブサイト (<https://www.jaea.go.jp>)
より発信されています。

国立研究開発法人日本原子力研究開発機構 研究開発推進部 科学技術情報課
〒319-1112 茨城県那珂郡東海村大字村松4番地49
E-mail: ird-support@jaea.go.jp

This report is issued irregularly by Japan Atomic Energy Agency.
Reuse and reproduction of this report (including data) is required permission.
Availability and use of the results of this report, please contact
Library, Institutional Repository and INIS Section,
Research and Development Promotion Department,
Japan Atomic Energy Agency.
4-49 Muramatsu, Tokai-mura, Naka-gun, Ibaraki-ken 319-1112, Japan
E-mail: ird-support@jaea.go.jp

Momentum Exchange Functions Model for SIMMER-III and SIMMER-IV

Yoshiharu TOBITA^{*1}, Satoru KONDO^{*2} and Tohru SUZUKI^{*3}

Fast Reactor Cycle System Research and Development Center
Oarai Research and Development Institute
Japan Atomic Energy Agency
Oarai-machi, Higashiibaraki-gun, Ibaraki-ken

(Received June 6, 2024)

The SIMMER-III and SIMMER-IV computer code, developed at the Japan Atomic Energy Agency (JAEA), is a two- and three-dimensional, multi-velocity-field, multi-component fluid-dynamics model, coupled with a space- and time-dependent neutron kinetics model. The codes have been used widely for simulating complex phenomena during core-disruptive accidents in liquid-metal fast reactors. In the multi-velocity-field fluid dynamics, momentum exchange functions (MXFs) are required for treating inter-field drag and fluid-structure friction effects and thereby for accurately simulating reactivity effects of relative motion of core materials.

Up to 8 velocity fields can be used in SIMMER-III and SIMMER-IV, with each field exchanging momentum with other fields and structure surfaces. Since both theoretical and experimental knowledge of the momentum exchange processes for a multi-component, multi-velocity flows is limited, the developed MXF formulations are based on engineering correlations of steady-state two-phase flows. Multi-phase flow regimes for both the pool and channel flows are modeled with using an appropriate averaging procedure such as to avoid abrupt changes in MXFs at flow regime transition.

The MXF model, together with the multi-phase flow topology and interfacial area model, has been extensively tested through the code assessment (verification and validation) program, which has demonstrated that many of the problems associated with limitation of two velocity fields and simplistic modeling in the previous codes were resolved.

Keywords: Multi-component Flow, Multi-phase Flow, Fluid Dynamics, Momentum Exchange Function, Drag and Friction, SIMMER-III, SIMMER-IV, V&V, Severe Accidents, CDA, LMFR Safety

*1 Karlsruhe Institute of Technology

*2 Fast Reactor Cycle System Research and Development Center until March 31, 2023

*3 Tokyo City University

SIMMER-III 及び SIMMER-IV コードの運動量交換関数モデル

日本原子力研究開発機構 大洗研究所 高速炉サイクル研究開発センター

飛田 吉春^{*1}、近藤 悟^{*2}、鈴木 徹^{*3}

(2024年6月6日受理)

日本原子力研究開発機構が開発した SIMMER-III 及び SIMMER-IV は、2次元及び3次元の多速度場・多成分流体力学モデルを空間・時間依存の核動特性モデルと結合した計算コードであり、液体金属高速炉の炉心崩壊事故の解析に広く利用されている。多速度場の流動解析においては、流体速度場間及び流体・構造壁間の抵抗や摩擦をモデル化した運動量交換関数 (MXF と呼ぶ) が必要となり、これにより熔融炉心物質間の相対運動や運動に伴う反応度効果が精度良く模擬される。

SIMMER-III 及び SIMMER-IV では最大 8 の速度場を使用でき、各速度場は他の速度場及び構造材壁と運動量を交換する。多成分・多速度場流体における運動量交換に関する理論的・実験的知見は限られているため、MXF の定式化は定常二相流に関する工学的相関式に基づいて行った。また、プール流及びチャンネル流における多相流流動様式のモデル化においては、適切な内挿手順を採用することにより流動様式の遷移における MXF の連続性を維持した。

MXF モデルは、多相流境界面積モデルと合わせて、コード検証 (V&V) プログラムを通じて幅広くテストを行った結果、従来のコードにおける 2 速度場の制約や簡易モデルに伴う問題点の多くを解決できることが示された。

大洗研究所：〒311-1393 茨城県東茨城郡大洗町成田町 4002 番地

*1 カールスルーエ工科大学

*2 高速炉サイクル研究開発センター (2023年3月31日迄)

*3 東京都市大学

Contents

1. Introduction.....	1
2. Overview of SIMMER-III and Purpose of Interfacial Areas.....	3
2.1. Overview of Fluid Dynamics Algorithm	3
2.2. SIMMER-III/SIMMER-IV Components.....	4
2.3. Purposes and Summary of Momentum Exchange Function Model.....	4
3. Momentum Field Quantities	6
3.1. Momentum Equation	6
3.2. Geometrical Variables	6
3.3. Viscosity	7
4. MXFs between Fluid Components	8
4.1. MXFs between Continuous and Discontinuous Fluids.....	8
4.2. MXFs between Discontinuous Components.....	9
4.3. MXFs between Continuous Components.....	10
4.4. Film Boiling around Hot Droplet or Particle	10
4.5. Effect of Bubble Shape on Drag Coefficient	11
4.6. Evaluation of Virtual Mass Term.....	13
5. MXFs between Fluid Components and Structure	14
5.1. Effective Particle Viscosity.....	14
5.2. MXFs between Continuous Fluid and Structure Components.....	15
5.3. MXFs between Dispersed Fluid and Structure Components	16
5.4. Special models in Fluid-Structure MXF	16
5.4.1. Introduction of Ueda’s model	16
5.4.2. Particle jamming model	16
5.4.3. Particle chunk model.....	17
6. Averaging of Momentum Exchange Functions	18
7. Verification and Validation.....	20
7.1. SIMMER-III Assessment Program.....	20
7.2. Results of Phase 1 Assessment	20
7.3. Results of Phase 2 Assessment	21
8. Conclusion	23
Acknowledgment.....	24
References.....	25
Appendix A Formulation of Particle Viscosity.....	32
1. Correlations for Effective Particle Viscosity	32
2. Experimental Data	33
3. Comparison of the Correlations with Experimental Data	33
4. Consideration.....	33
Appendix B Ueda’s Model	35
Appendix C Particle Chunk Model.....	39

目 次

1. 序論	1
2. SIMMER-III 概要及び境界面積モデルの目的	3
2.1. SIMMER-III の流体力学モデル	3
2.2. SIMMER-III/SIMMER-IV の成分	4
2.3. 運動量交換関数モデルの目的と概要	4
3. 運動量場に関わる変数	6
3.1. 運動量方程式	6
3.2. 幾何形状に関わる変数	6
3.3. 粘性係数	7
4. 流体成分間の運動量交換関数	8
4.1. 連続流体－分散流体間の運動量交換関数	8
4.2. 分散流体間の運動量交換関数	9
4.3. 連続流体間の運動量交換関数	10
4.4. 高温液滴又は粒子の周りの膜沸騰	10
4.5. ドラグ係数に対する気泡形状の効果	11
4.6. 仮想質量	13
5. 流体成分－構造材間の運動量交換関数	14
5.1. 実効粒子粘性	14
5.2. 連続流体－構造材間の運動量交換関数	15
5.3. 分散流体－構造材間の運動量交換関数	16
5.4. 特別なモデル	16
5.4.1. 上田モデルの導入	16
5.4.2. 粒子ジャミングモデル	16
5.4.3. 粒子チャンクモデル	17
6. 運動量交換関数の平均化	18
7. モデル検証及び妥当性評価	20
7.1. SIMMER-III の検証プログラム	20
7.2. 第 1 期検証の結果	20
7.3. 第 2 期検証の結果	21
8. 結論	23
謝辞	24
参考文献	25
付録 A：粒子粘性の定式化	32
1. 実効粒子粘性の相関式	32
2. 実験データ	33
3. 相関式と実験データの比較	33
4. 考察	33
付録 B：上田モデル	35
付録 C：粒子チャンクモデル	39

Nomenclature

Symbols

$A_{qq'}, B_{qq'}$	Laminar and turbulent terms of momentum exchange function between velocity fields q and q'
A_{qS}, B_{qS}	Laminar and turbulent terms of momentum exchange function between velocity field q and structure
A_{pj}	Maximum packing fraction used in the particle jamming model
a	Binary contact area
B_{pj}	Fraction of A_{pj} above which the particle jamming model is applied
C_D	Drag coefficient
C_G	Virtual mass coefficient
C_{pj}	Exponent in the particle jamming model which is used to calculate MXF increase
C_{PVIS}	Adjusting parameter in the particle viscosity formulation
C_{PVS1}, C_{PVS2}	Parameters to determine the shape of weighting function Ψ
D_h	Hydraulic diameter
D_H^*	Dimensionless hydraulic diameter
Eo	Eötvös number
f	Friction factor
g	Gravity acceleration
H	Heaviside function
K	Momentum exchange function
Mo	Morton number
$N_{\mu f}$	Viscosity number
P	Pressure
Q_N	Nuclear heat generation rate
Re	Reynolds number
r	Radius
r_{CL}	Characteristic particle radius
r_{Ln}	Particle radii for $Ln=4, 5, 6$ and 7
S_f	Multiplication factor for the molecular viscosity coefficient
VM	Virtual mass
\vec{v}	Velocity (vector)
X_D	Fraction of liquid components in vapor-continuous region

Greek symbols

α	Volume fraction
----------	-----------------

$\alpha_{G,eff}$	Effective void fraction
$\alpha_{G,EOS}$	Real void fraction
Γ	Mass transfer rate
μ	Viscosity
Ψ	Weighing function
τ	Time constant
φ	Increment of momentum exchange function in particle jamming model
ρ	Microscopic density
$\bar{\rho}$	Macroscopic density
σ	Surface tension

Subscripts and superscripts

B	Bubbly flow region
CL	Continuous liquid
CP	Continuous phase
D	Dispersed flow region
F	Flow
f	Fluid, liquid
G, g	Vapor, gas
L	Liquid
m	m-th density component
M	M-th energy component
MP	Maximum packing
n	n-th density component
P	Particle
PIN	Fuel pin
q	q-th velocity field (momentum component)
S	Structure

1. Introduction

The computer codes SIMMER-III/SIMMER-IV couple a two-/three-dimensional, multi-velocity field, multi-phase, multi-component, Eulerian fluid dynamics module with a space- and time-dependent neutronics model and a structure model.¹⁾⁻⁷⁾ In order to model complex multi-phase flow physical processes, mass and energy conservation equations are solved for the density and energy components, respectively. The three-dimensional SIMMER-IV code retains essentially the same modeling as the two-dimensional SIMMER-III, except for the fluid convection algorithm and the additional structure wall treatment in SIMMER-IV. In the remainder of this report, only the code name SIMMER-III is referred to in many places, unless otherwise noted.

The SIMMER-III and SIMMER-IV codes are used for simulating dynamic and complex physical processes of multi-phase flows during core disruptive accidents (CDAs) in a liquid-metal fast reactor (LMFR), such as boiling pool dynamics, molten fuel relocation and freezing, and fuel-coolant interactions, by solving time-dependent mass, momentum and energy equations. These are the phenomena occurring through heat, mass and momentum transfer processes at the interfaces between different materials (or components). For momentum transfer, the momentum exchange functions (MXFs) are formulated to describe the momentum exchange processes occurring at the fluid-fluid and fluid-structure interfaces.

In the former SIMMER-II code⁸⁾ developed at the Los Alamos National Laboratory, a two-velocity code, only a dispersed droplet flow regime is assumed, and the liquid-vapor drag force and the liquid- and vapor-structure friction forces are modeled as MXFs. In the three-velocity-field AFDM code^{9),10)}, a solution approach to simulate relative motion of light and heavy liquids was successfully implemented. SIMMER-III is an extension of the AFDM approach up to 8 velocity fields, to each of which 8 fluid energy components (7 liquids and 1 vapor mixture) can be freely assigned. The MXFs are extended accordingly, and in addition an enhanced multi-phase flow topology and interfacial area model (IFA) is fully taken into consideration.

Since both theoretical and experimental knowledge of the momentum exchange processes for a multi-component multi-velocity flow is limited, the developed formulations are based on engineering correlations of steady-state two-phase flows. In SIMMER-III, fluid-structure friction, fluid-fluid drag and liquid-vapor virtual mass effects are modeled. Although the MXFs and the virtual mass coefficient are actually used to solve the momentum equation in the fluid dynamics convection algorithm, they are evaluated as a part of the intra-cell transfer (Step 1) after the multi-phase flow regimes and interfacial areas are updated.

In this report, the fluid dynamics model of SIMMER-III is briefly presented in Chapter 2 to understand the purpose and importance of the MXF model. The basic formulation of the MXF, the definition and the averaging procedure of the physical parameters for each velocity field are described in Chapter 3. The MXF between fluid components and the MXF between fluid components and structure are described in Chapters 4 and 5, respectively. Chapter 6 briefly describes the description of the averaging procedure of the MXFs in each momentum component field. Although the detailed discussion of the verification and validation (V&V) is beyond the scope of this report, the achievements of SIMMER-III assessment program with respect to

MXF modeling are summarized in Chapter 7. Additional detailed information with respect to the MXF modeling is available in Appendices.

2. Overview of SIMMER-III and Purpose of Interfacial Areas

2.1. Overview of Fluid Dynamics Algorithm

The fundamental mass, momentum and energy equations are written in a differential form as follows. For mass conservation,

$$\frac{\partial \bar{\rho}_m}{\partial t} + \nabla \cdot (\bar{\rho}_m \vec{v}_q) = -\Gamma_m, \quad (2-1)$$

where the mass is represented by the macroscopic density (mass per unit volume) $\bar{\rho}_m$ and Γ_m is the total mass-transfer rate per unit volume from component m . The momentum conservation equation is written as:

$$\begin{aligned} \frac{\partial \bar{\rho}_q \vec{v}_q}{\partial t} + \sum_{m \in q} \nabla \cdot (\bar{\rho}_m \vec{v}_q \vec{v}_q) + \alpha_q \nabla p - \bar{\rho}_q \vec{g} + K_{qS} \vec{v}_q - \sum_{q'} K_{qq'} (-\vec{v}_q) - \mathbf{VM}_q \\ = - \sum_{q'} \Gamma_{qq'} [H(\Gamma_{qq'}) \vec{v}_q + H(\Gamma_{q'q}) \vec{v}_{q'}], \end{aligned} \quad (2-2)$$

where the K_{qS} and $K_{qq'}$ terms on the left side \vec{v}_q are the MXFs that couple the velocity field q to a different field or structure, and \mathbf{VM}_q is the virtual mass term. The energy conservation equation is written below, where the energy is represented by the specific internal energy of component M .

$$\begin{aligned} \frac{\partial \bar{\rho}_M e_M}{\partial t} + \sum_{m \in M} \nabla \cdot (\bar{\rho}_m e_m \vec{v}_q) + p \left[\frac{\partial \alpha_M}{\partial t} + \nabla \cdot (\alpha_M \vec{v}_q) \right] \\ - \frac{\bar{\rho}_M}{\bar{\rho}_m} \left[\sum_q K_{q'q} (\vec{v}_q - \vec{v}_{q'}) \cdot (\vec{v}_q - \vec{v}_{q'}) + K_{qS} \vec{v}_q \cdot (\vec{v}_q - \vec{v}_{qS}) + \mathbf{VM}_q \right. \\ \left. \cdot (\vec{v}_q - \vec{v}_{GL}) \right] = Q_N + Q_M(\Gamma_M) + Q_H(h, a, \Delta T), \end{aligned} \quad (2-3)$$

where the terms on the right-hand side of the equation denote the specific energy sources due to nuclear heating, mass transfer, and heat transfer to the energy component M . The detailed explanation of these equations is described in the SIMMER-III/SIMMER-IV manual.¹⁾

The most complex portion of the fluid dynamics is the model for intra-cell heat and mass transfer model, which describes the physical phenomena associated with multi-component, multiphase flows. Interactions between different components having different energies take place locally at places where two components come into contact. In the former SIMMER-II, the heat and mass exchange rates were determined at the beginning of time step, and updates at the end-of-time-step due to convection were calculated assuming that these exchange rates stayed constant during the time step. The approach taken by SIMMER-II is merited when relatively large time steps sizes can be used for quasi-steady-state problems. However, for highly transient cases with rapid phase transitions, non-linear phenomena such as vaporization and condensation cannot be treated accurately and consistently. In the past, this limitation of the code has caused serious stability and accuracy problems.

The fundamental fluid-dynamics solution algorithm employed in SIMMER-III is the time-factorization, four-step method, first developed for the AFDM code, in which intra-cell transfer is decoupled from fluid convection. The complexity associated with modeling the various interrelated phenomena of heat and mass transfer is the main reason for choosing this approach. Based on the successful implementation of the algorithm in AFDM, the same solution procedure is adopted in SIMMER-III/SIMMER-IV with an extension to multi-component systems with full reactor materials and structure configuration. In the four-step algorithm, local phenomena or interactions are treated as intra-cell transfer processes in Step 1, which is decoupled from the fluid inter-cell convection treated in Steps 2-4. Step 1 solves the mass and energy equations without convection terms, and updates the mesh cell variables at the end of the time step resulted from intra-cell heat and mass transfer. Also evaluated in Step 1 are momentum exchange functions to be used in fluid-convection calculations. The individual models of Step 1 are programmed in a modular way such that future improvement or replacement with new models can be implemented easily.

2.2. SIMMER-III/SIMMER-IV Components

All materials are represented by components: density components are used to calculate the mass conservation equations; and energy components the energy conservation equations. The complete lists of the structure-, liquid- and vapor-field components are shown in Tables 1 through 3. In these tables, the lower-case subscripts denote density components while the upper-case subscripts denote energy components. The fuel components are divided into fertile and fissile in their mass (density components) to represent different fuel enrichment zones in the core. However, the two fuel components are assumed to be intimately mixed, and therefore assigned a single temperature (energy components). It is noted that the only difference between SIMMER-III and SIMMER-IV is the number of can walls; i.e. the front and back can walls are modeled in a three-dimensional code in addition to the left and right can walls.

With respect to the velocity fields, the three-velocity-field fluid dynamics was initially developed. There are seven liquid-field energy components and one vapor mixture in SIMMER-III. The assignment of the eight fluid energy components to the three velocity fields ($q1$, $q2$ and $q3$) is shown in Tables 2 and 3. Of the two liquid-field velocity fields, $q1$ represents heavier components and $q2$ lighter components.

The limitation of three velocity fields was relaxed in the later model enhancement to flexibly assign the fluid energy components to different velocity fields. This means the maximum number of the velocity fields is eight (seven liquid components and one vapor mixture), although the standard and default number of velocity fields is still three. The recommended 6-velocity-field assignment for an LMFR simulation is also shown in Tables 2 and 3 as well. An increase of the velocity fields required significant model enhancement effort to solve up to 8 momentum equations and to increase the fluid-to-fluid drag terms from 1 for SIMMER-II⁸⁾ or 3 for AFDM¹⁰⁾ to up to 28.

2.3. Purposes and Summary of Momentum Exchange Function Model

The SIMMER-III/SIMMER-IV fluid dynamics solves the mass, momentum and energy equations in multi-component, multi-velocity-field systems. The MXFs appearing in the momentum equation model a drag force between a pair of velocity fields and a friction force between a structure and a velocity field. Although the modeling concept is similar to the two-velocity SIMMER-II and three-velocity AFDM, the

treatment in SIMMER-III/SIMMER-IV has become much more complex, because up to eight velocity fields can be used with allowing flexible assignment of liquid components to any velocity fields and the channel flow regimes are modeled in addition to the pool flow regimes in the previous codes. Hence, the MXF model can adequately simulate the relative motions of fluid components of different densities, taking into account the local multiphase flow topology.

In the solution algorithm, the intra-cell mass, momentum and energy transfer terms are solved in Step 1, for which a simplified computational flow is depicted in Fig. 1. Although the MXFs and the virtual mass coefficient are actually used in solving the momentum equation in the fluid dynamics convection algorithm in Steps 2 through 4, they are evaluated as a part of Step 1 after the multi-phase flow regimes and interfacial areas are updated. Similar to the heat transfer coefficient model, the MXF model covers a whole scope of pool and channel flow maps. Based on the structure configuration and component volume fractions, a flow regime is determined in each mesh cell. Binary contact areas are determined between pairs of energy components for fluid-fluid and fluid-structure interfaces. Binary contact areas are then summed over each velocity field to evaluate MXFs between a velocity field (momentum component) and other velocity fields or structure.

There are several specific features in the SIMMER-III/SIMMER-IV MXF model. First, virtual mass terms are included based on the previous AFDM code. Second, the effects of solid particles on flow resistance are modeled by defining effective viscosity for particles. Depending on a geometrical limitation, blockage formation of a flow channel can be simulated as well. Third, a special empirical model has been implemented to simulate the effect of turbulence enhancement at the liquid-gas interface on pressure drop.

3. Momentum Field Quantities

3.1. Momentum Equation

The momentum equation presented in Eq. (2-2) includes the momentum coupling terms called momentum exchange functions (MXFs). The MXF between velocity fields q and q' , which appears as $K_{qq'}$, describes the rate of momentum exchange per unit volume after being multiplied by the velocity difference between the two velocity fields. The MXF between the velocity field q and structure, K_{qS} , which is multiplied by velocity, gives the frictional loss by the structure. The MXF is a function of the drag coefficient and the interfacial areas and consists of laminar and turbulent terms,

$$K_{qq'} = A_{qq'} + B_{qq'} |\vec{v}_{q'} - \vec{v}_q|. \quad (3-1)$$

for the MXF between velocity fields. The first term $A_{qq'}$ is described by Stoke's law, and the turbulent term $B_{qq'} |\vec{v}_{q'} - \vec{v}_q|$ is proportional to the inter-phase velocity difference with the drag coefficient. Similarly, the MXF between velocity field q and structure S consists of the laminar and turbulent terms,

$$K_{qS} = A_{qS} + B_{qS} |\vec{v}_q|. \quad (3-2)$$

3.2. Geometrical Variables

To formulate the MXFs between two velocity fields, it is necessary to calculate the geometric variables such as the interfacial area and volume fractions of each momentum component. The volume fractions of each momentum component are calculated simply by summing the volume fractions of the energy components belonging to the momentum field as follows:

$$\alpha_{qm} = \sum_{Lm \in qm} \alpha_{Lm}, \quad (3-3)$$

$$\alpha_{qm,B1} = \sum_{Lm \in qm} \alpha_{Lm,B1}, \quad (3-4)$$

$$\alpha_{qm,B2} = \sum_{Lm \in qm} \alpha_{Lm,B2}, \text{ and} \quad (3-5)$$

$$\alpha_{qm,D} = \sum_{Lm \in qm} \alpha_{Lm,D}, \quad (3-6)$$

where $B1$, $B2$ and D denotes the quantities in the first bubbly flow region, the second bubbly flow region and dispersed flow region.

Since the MXFs are calculated for each energy component, the binary contact areas in each flow region are not summed to the binary contact areas between the momentum components except for the binary contact areas at the interface of the bubbly flow region and the dispersed flow region,

$$\alpha_{qm,qn,l} = \sum_{Lm \in qm, Ln \in qn} \alpha_{Lm, Ln, l} \cdot \quad (3-7)$$

3.3. Viscosity

The viscosity of each momentum component is not currently used to evaluate MXFs, but is calculated as a part of MXF modeling, because it is used in the later part of the SIMMER-III code.

$$\mu_{qm} = \sum_{Lm \in qm} \alpha_{Lm} / \sum_{Lm \in qm} \frac{\alpha_{Lm}}{\mu_{Lm}} \quad \text{for } Lm=1, 2, 3. \quad (3-8)$$

The viscosity of a mixture of liquid and solid particles becomes larger than the viscosity of the pure liquid component due to the momentum dissipation caused by the collision and friction between the solid particles. In order to simulate this increase of effective mixture viscosity, μ_{qm} is multiplied by a factor:

$$S_f = \sum_{Lm \in qm} \alpha_{Lm} / \left(\sum_{Lm \in qm} \alpha_{Lm} + \sum_{Ln \in qn} \alpha_{Ln} \right) + C_{PVIS} \alpha_{MP} \sum_{Ln \in qn} \alpha_{Ln} / \left[\alpha_{MP} \left(\sum_{Lm \in qm} \alpha_{Lm} + \sum_{Ln \in qn} \alpha_{Ln} \right) - \sum_{Ln \in qn} \alpha_{Ln} \right], \quad (3-9)$$

for $Lm=1, 2, 3$ and $Ln=4, 5, 6, 7$

4. MXFs between Fluid Components

4.1. MXFs between Continuous and Discontinuous Fluids

The MXFs between continuous liquid component and discontinuous component such as bubbles, droplets and particles are modeled based on Ishii's drag-similarity hypothesis¹¹⁾, which assumes that the drag in a multiparticle system follows the same Reynolds number function as isolated spherical bubbles or droplets using a modified viscosity. The existence of other droplets or particles in the continuous liquid component is accounted for by calculating the effective viscosity (particle viscosity) of the continuous mixture surrounding the droplet or particle component. The current model uses the following formulation,

$$\mu_c = \left(\alpha_L / \sum_{Lm=1, Lm \neq D}^3 \frac{\alpha_{Lm}}{\mu_{Lm}} \right) \left[\frac{\alpha_L}{\alpha_L + \alpha_P} + C_{PVIS} \frac{\alpha_{MP} \alpha_P}{\alpha_{MP} (\alpha_L + \alpha_P) - \alpha_P} \right], \quad (4-1)$$

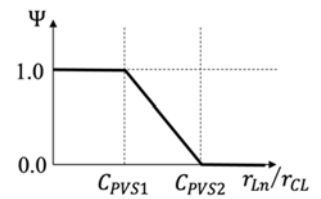
where C_{PVIS} is the adjusting parameter in the particle viscosity formulation, and

$$\alpha_L = \sum_{Lm=1, Lm \neq D}^3 \alpha_{Lm} \quad \text{and} \quad \alpha_P = \sum_{Ln=4, Ln \neq D}^7 \Psi(r_{Ln}/r_{CL}) \alpha_{Ln},$$

The index D denotes the discontinuous droplet or particle component that exchanges momentum with the continuous mixture. In summing the volume fractions of solid particle components ($Ln=4, 5, 6$ and 7), the volume fractions of each component are multiplied by a weighing function:

$$\Psi(r_{Ln}/r_{CL}) = \max \left[0, \min \left(1, \frac{r_{Ln}/r_{CL} - C_{PVS1}}{C_{PVS2} - C_{PVS1}} \right) \right] \quad \text{for } C_{PVS1} < C_{PVS2}, \quad (4-2)$$

The particle viscosity model assumes that the solid particles are small enough for the mixture to be regarded as a continuum. When the size of solid particles becomes larger than a certain characteristic length, these solid particles are no longer considered to form a continuum and should be excluded from the summation in the particle viscosity model. This function is used to optionally model this effect. The parameter r_{CL} is the characteristic particle radius (default value 2.5×10^{-3}), and C_{PVS1} and C_{PVS2} are the threshold values in the graph of $\Psi(r_{Ln}/r_{CL})$ shown right. With the default values of C_{PVS1} and C_{PVS2} of 0.5×10^{20} and 1.0×10^{20} , respectively, this function has no effect on the summation.



The MXF between the droplet or particle and the continuous liquid component is defined using Ishii's drag-similarity hypothesis¹¹⁾ as follows:

$$\mu^+ = \frac{\mu_D + 0.4\mu_c}{\mu_D + \mu_c}, \quad (4-3)$$

$$\mu_a = \mu_c \left[\max \left(1 - \frac{\alpha_{D,B1}}{\alpha_{dm} f_{B1} \alpha_{F,S}}, 1.0 \times 10^{-10} \right) \right]^{-2.5 \alpha_{dm} \mu^+}, \quad (4-4)$$

$$\text{Re} = \frac{2r_{D,B1}\rho_c|v_c - v_D|}{\mu_c}, \quad (4-5)$$

$$r_D^* = r_{D,B1} \left(\frac{\sigma_c g(\rho_c - \rho_D)}{\mu_c^2} \right)^{1/3}, \quad (4-6)$$

$$\mu^* = \frac{\mu_c}{\sqrt{\rho_c |\sigma_c - \sigma_D| \sqrt{g(\rho_c - \rho_D)}}}, \quad (4-7)$$

$$\Psi = 0.55 \left[(1 + 0.08(r_D^*)^3)^{4/7} - 1 \right]^{0.75}, \quad (4-8)$$

$$F = \frac{\mu_c}{\mu_a} \sqrt{\frac{\alpha_{D,B1}}{f_{B1} \alpha_{F,B}}}, \quad (4-9)$$

$$C_D^* = \begin{cases} \frac{4}{3} r_{D,B1} \sqrt{\left| \frac{g(\rho_c - \rho_D)}{\sigma_c - \sigma_D} \right|} \left[\frac{1 + 17.67F^{6/7}}{18.67F} \right]^2 & \text{for } \mu^* \geq 0.11 \frac{1 + \Psi}{\Psi^{8/3}} \\ 0.45 \left[\frac{1 + 17.67F^{6/7}}{18.67F} \right]^2 & \text{for } \mu^* < 0.11 \frac{1 + \Psi}{\Psi^{8/3}} \end{cases}, \quad (4-10)$$

$$C_D^+ = 2.4 \text{Re}^{0.25}, \quad (4-11)$$

$$C_D = C_{CD} \max(C_D^+, C_D^*), \quad (4-12)$$

$$A_{C,D,B1} = \frac{3}{2} a_{C,D,B1} \frac{\mu_a}{r_{D,B1}}, \text{ and} \quad (4-13)$$

$$B_{qC,qD,B1} = \frac{a_{qC,qD,B1} C_D}{2} \frac{C_D}{4} \rho_{qC}. \quad (4-14)$$

The MXF between bubble and continuous liquid, or the MXF between droplet and continuous vapor is defined by expressions similar to Eqs. (4-13) and (4-14), where the physical values of corresponding component are replaced by those of the vapor.

4.2. MXFs between Discontinuous Components

The two discontinuous components are assumed to slide against each other during the time they are in contact, exchanging momentum by friction. An average density is used to refer to a single boundary layer between the discontinuous phases. The MXFs between discontinuous components assume a constant drag coefficient and are given by

$$A_{D1,D2,B1} = 0, \text{ and} \quad (4-15)$$

$$B_{D1,D2,B1}=0.01C_{dd}a_{D1,D2,B1}\frac{\bar{\rho}_{D1,B1}+\bar{\rho}_{D2,B1}}{\alpha_{D1,B1}+\alpha_{D2,B1}}. \quad (4-16)$$

Here, the default drag coefficient is 0.01 recommended by Bohl⁸⁾ and the user-defined constant C_{dd} is used to represent the large uncertainty associated with the definition of this MXF.

4.3. MXFs between Continuous Components

The MXFs between continuous components (continuous liquid and vapor) assume a constant drag coefficient and are given by

$$A_{CP,G}=0, \text{ and} \quad (4-17)$$

$$B_{CP,G}=C_{cc}a_{CP,G}\frac{\rho_G}{2}, \quad (4-18)$$

where $a_{CP,G}$ is the interfacial area between continuous phases and $C_{cc} = 0.005$ is recommended for SIMMER-III.

4.4. Film Boiling around Hot Droplet or Particle

When a hot droplet or particle (“particle” is used throughout this section) moves in coolant, it is surrounded by thin vapor film if the temperature is higher than the minimum film boiling temperature, which depends on the thermophysical properties and ambient pressure. The hot particle does not come into direct contact with the coolant liquid, since the particle surface is covered by vapor, which is continuously generated from the coolant liquid-vapor interface and flows inside the film from the bottom to the top around the particle. It is the vapor flowing inside the film that gives a resistance to the moving particle. The usual drag correlation cannot account for such a configuration.

The drag coefficient between a particle and coolant liquid under the film boiling condition was developed by Cao and Tobita¹²⁾ and is given by

$$C_D=a_0(1-a_p)^{2n}+a_1\frac{Ev\mu_0}{Re\rho_0}(1-a_p)^{2n}+a_2\left(\frac{Ev\mu_0^2}{g_0\rho_0}\right)^{1/3}(1-a_p)^{2n}+a_3\frac{g_0}{Re^2}+\frac{1}{Ev}(1-a_p)^{2n}, \quad (4-19)$$

for $Re < 2000$, and

$$C_D=w_0(1-a_p)^{2n}+w_1\frac{Ev\mu_0}{Re\rho_0}(1-a_p)^{2n}+w_2\left(\frac{Ev\mu_0^2}{g_0\rho_0}\right)^{1/3}(1-a_p)^{2n}+w_3\frac{g_0}{Re^2}, \quad (4-20)$$

for $Re \geq 2000$, where the dimensionless numbers are

$$g_0=\frac{D_D^3\rho_c^2g}{\mu_c^2}, \quad \mu_0=\frac{\mu_{vapor}}{\mu_c}, \quad \rho_0=\frac{\rho_{vapor}}{\rho_c},$$

and evaporation number Ev is defined by

$$Ev = \frac{\Gamma D_D}{\mu_{vapor}},$$

where Γ is the evaporation mass flux at the surface of particle. The coefficients in Eq. (4-19) are determined so that the equation fits well with the theoretical formulation as, $a_0 = 0.849$, $a_1 = 2.05 \times 10^{-3}$, $a_2 = 3.47$, $a_3 = 4.24 \times 10^{-2}$, $w_0 = 6.5 \times 10^{-3}$, $w_1 = 6.89 \times 10^{-2}$, $w_2 = 1.1 \times 10^{-2}$ and $w_3 = 5.11$. This correlation was applied to an analysis of the QUEOS experiment¹³⁾ and showed good agreement with experimental results by improving the drag correlation under the film-boiling condition using Eqs. (4-19) and (4-20).

4.5. Effect of Bubble Shape on Drag Coefficient

In the two-phase bubble column experiments with high liquid-gas density ratio flows, deformed ellipsoidal bubbles were identified at lower gas velocities, but at higher gas velocities the spherical cap bubbles were observed¹⁴⁾. The analysis of this experiment showed that the original momentum exchange model is appropriate for ellipsoidal bubbly flows with lower void fraction, and that the accuracy of SIMMER-III for cap bubbly flows with higher void fraction is significantly improved with Kataoka-Ishii's correlation^{15), 16), 17)}. In addition, a new procedure was developed to automatically select an appropriate drag coefficient depending on the bubble shape.

To take the bubble shape into account, the following equation proposed by Ishii and Chawla¹⁸⁾ was used to calculate the drag coefficient of spherical cap bubbles:

$$C_D = \frac{8 r_b g \Delta \rho (1 - \alpha_S)}{3 \rho_f v_{gr}^2}, \quad \text{where } v_{gr} = \frac{v_{gl}}{1 - C_0 \alpha}, \quad (4-21)$$

and v_{gl} and C_0 are the drift velocity and the distribution parameter, respectively. Kataoka and Ishii¹⁵⁾ proposed to evaluate these parameters based on various experimental data with ordinary flows containing cap bubbles in a pool. Thus v_{gl} is given by

$$v_{gl} = 0.0019 D_H^{*0.809} \left(\frac{\rho_g}{\rho_f} \right)^{-0.157} N_{\mu f}^{-0.562} \left(\frac{\sigma g \Delta \rho}{\rho_f} \right)^{0.25}, \quad (4-22)$$

for $D_H^* \leq 30$ and $N_{\mu f} \leq 2.2 \times 10^{-3}$, or

$$v_{gl} = 0.030 D_H^{*-157} \left(\frac{\rho_g}{\rho_f} \right)^{-0.157} N_{\mu f}^{-0.562} \left(\frac{\sigma g \Delta \rho}{\rho_f} \right)^{0.25}, \quad (4-23)$$

for $D_H^* > 30$ and $N_{\mu f} \leq 2.2 \times 10^{-3}$, and C_0 is given by

$$C_0 = 1.35 - 0.35 \sqrt{\frac{\rho_g}{\rho_f}}, \quad \text{for a rectangular channel, and} \quad (4-24)$$

$$C_0 = 1.2 - 0.2 \sqrt{\frac{\rho_g}{\rho_f}}, \quad \text{for a round tube.} \quad (4-25)$$

In Eqs. (4-22) and (4-23), D_H^* and $N_{\mu f}$ are the dimensionless hydraulic diameter and the viscosity number, respectively, and defined as

$$D_H^* = \frac{D_H}{\sqrt{\sigma/g\Delta\rho}}, \text{ and} \quad (4-26)$$

$$N_{\mu f} = \frac{\mu_f}{(\rho_f \sigma \sqrt{\sigma/g\Delta\rho})^{1/2}}. \quad (4-27)$$

In the implementation of this formulation in SIMMER-III, it is important to select the appropriate drag coefficient according to the bubble shape in the bubbly flow regime. For lower gas velocities or lower void fractions, the C_D expressed by Eq. (4-12) should be used for ellipsoidal bubbly flow. For higher gas velocities or higher void fractions, C_D given by Eq. (4-21) for cap bubble flow would greatly improve the accuracy of SIMMER-III with respect to cap bubbly flows. To adequately represent this situation, a revised pool flow regime map is proposed as shown in Fig. 3, instead of Fig. 2. In the bubbly flow regime, the volume fraction of a cap bubbly flow region increases with increasing void fraction. In the transition flow regime, the flow is regarded as a mixture of cap bubbly flow and droplet flow. To simplify the procedure, the drag coefficient in a mixture of ellipsoidal bubbly flow and cap bubbly flow is interpolated using a simple exponential function as

$$C_D = C_{D,ellipsoidal}\{\exp(F\alpha)\} + C_{D,cap}\{1 - \exp(F\alpha)\}, \quad (4-28)$$

where $C_{D,ellipsoidal}$ is the drag coefficient of an ellipsoidal bubble given by Eq. (4-12), and $C_{D,cap}$ is that of a cap bubble given by Eq. (4-21). The parameter F is assumed to be expressed as a function of dimensionless group:

$$F = F(\text{Re}, \text{Eo}, \text{M}), \quad (4-29)$$

where Re , Eo and M are Reynolds, Eötvös and Morton numbers, respectively, which are often used to describe the property of a bubble.

A bubble-shape map proposed by Grace^{19), 20)} and Crif²¹⁾ and is shown in Fig. 4. The bubble shapes are roughly divided into three types according to the dimensionless numbers. The boundary between the ellipsoidal bubble and the cap bubble is simply defined by $\text{Eo} = 40$ for comparatively large Reynolds number. This means that the deformed ellipsoidal bubble can be seen in the case with $\text{Eo} < 40$, and the spherical cap bubble appears where $\text{Eo} > 40$. Therefore, Eq. (4-29) can be rewritten as:

$$F = F(\text{Eo}). \quad (4-30)$$

Furthermore, in order to generalize the effect of the flow property, the following conditions should be satisfied: C_D approaches $C_{D,ellipsoidal}$ for suitably small Eo , i. e. low-liquid-density or ordinary flows including ellipsoidal bubbles; and C_D approaches $C_{D,cap}$ for suitably large Eo , i. e. high-liquid-density flows including only cap bubbles. Comparing these conditions with Eq. (4-29), one can obtain

$$\begin{cases} F \rightarrow 0 & \text{for small Eo : } C_D \rightarrow C_{D,ellipsoidal} \\ F \rightarrow \infty & \text{for large Eo : } C_D \rightarrow C_{D,cap} \end{cases}, \quad (4-31)$$

and the following correlation is proposed for F :

$$F=1 - \exp(0.084Eo) , \quad (4-32)$$

such that the volume fraction of cap bubbly flow is 0.5 at $Eo=40$.

Figure 5 shows the result of the code improvement using Eq. (4-24) with Eq. (4-28). Open circles and squares in this figure show the calculated results with drag coefficients for ellipsoidal bubble and cap bubble, respectively. Closed diamonds show the results of the improved SIMMER-III, which are in reasonable agreement with the experimental results given by open diamonds. It is seen that the calculated results with Eq. (4-24) is shifted smoothly from those of the ellipsoidal bubble to the cap bubble with increasing superficial gas velocity.

4.6. Evaluation of Virtual Mass Term

The basic concept of a virtual mass force can be understood by considering the change in kinetic energy of the fluid surrounding an accelerating sphere. The classical solution for a realistic fluid without viscosity is that the acceleration of the sphere induces a resisting force on the sphere equal to one-half the mass of the displaced fluid times the acceleration of the sphere. Bohl gave an extensive literature survey on the effect of a virtual mass and derived the functional form in AFDM in order to improve the numerical stability. The physical background and the purpose of the implementation of the model are discussed in Appendix A of the AFDM manual Vol. V⁽²²⁾. The same model as AFDM is implemented in SIMMER-III/SIMMER-IV. The virtual mass coefficients are evaluated in Step 1 and are actually used in Steps 2 and 4.

The virtual mass term in each momentum field is given by

$$\mathbf{VM}_{q \notin G} = -\alpha_{q,eff} , \text{ and} \quad (4-33)$$

$$\mathbf{VM}_G = -\alpha_G \bar{\rho}_{eff} C_G \frac{\alpha_L}{\alpha_L + \alpha_P} \left[\frac{\partial \mathbf{v}_G}{\partial t} - \sum_{q \notin G} \alpha_{q,eff} \frac{\partial \mathbf{v}_q}{\partial t} \right] , \quad (4-34)$$

where the virtual mass coefficient C_G is defined as,

$$C_G = \begin{cases} \frac{1}{2} \left(1 + \frac{2\alpha_{G,eff}}{1 - \alpha_{G,eff}} \right) & \text{for } \alpha_{G,eff} \leq \frac{1}{2} \\ 2 \left(\frac{\alpha_D - \alpha_{G,eff}}{\alpha_D - 1/2} \right)^2 & \text{for } \frac{1}{2} < \alpha_{G,eff} \leq \alpha_D \\ 0 & \text{for } \alpha_D < \alpha_{G,eff} \end{cases} \quad (4-35)$$

5. MXFs between Fluid Components and Structure

Since the experimental knowledge of the frictional loss in multi-phase flow is limited, the MXFs between continuous liquid component and structure are defined by the analogy to the correlations for the ordinary two-phase flows. The basic idea to define the MXF between a component in a multi-component multi-phase flow and a structure surface is to regard the flow as a combination of single-phase flow in a separate pipe. The hydraulic diameter of each pipe is calculated from the volumetric fraction and binary contact area of each component,

$$D_h = \frac{4\alpha_{Lm}}{a_{Lm,S}}. \quad (5-1)$$

5.1. Effective Particle Viscosity

There are two models in the particle viscosity model for the MXFs between fluid components and structure surfaces and these models are selected by specifying the input flag MXFOPT(7). The first model (MXFOPT(7)=0) is similar to the particle viscosity model in the previous chapter and the multiplication factor for the molecular viscosity coefficient of the continuous liquid component is given by

$$S_f = \frac{\alpha_L}{\alpha_L + \alpha_P} + C_{PVIS} \frac{\alpha_{MP}\alpha_P}{\alpha_{MP}(\alpha_L + \alpha_P) - \alpha_P}, \quad (5-2)$$

where

$$\alpha_L = \sum_{Lm=1}^3 \alpha_{Lm} \quad \text{and} \quad \alpha_P = \sum_{Ln=4}^7 \Psi(r_{Ln}/r_{CL})\alpha_{Ln},$$

and the volume fractions of solid particles ($Ln=4, 5, 6, 7$) are multiplied by weighing function $\Psi(r_{Ln}/r_{CL})$ defined in Eq. (4-2). This formulation represents the physical consideration that the effective viscosity of multi-phase mixture should increase as the volume fraction of solid particles in it increases. Since it is assumed that the solid particles are dispersed in the continuous liquid, this equation is applied only to the continuous liquid component and does not change the effective viscosity of dispersed droplets. For the solid particle components, the multiplication factor is given as follows,

$$S_f = 1 + C_{PVIS} \frac{\alpha_{MP}\alpha_P}{\alpha_{MP}(1 - \alpha_S) - \alpha_P}, \quad (5-3)$$

where α_S is the sum of volume fractions of structure components. This formula implies that the mixture of liquid and solid particle may form a blockage if the volume fraction of particles in the flow area approaches the maximum packing fraction.

The second model (MXFOPT(7)=1) was introduced to SIMMER-III so as to better represent the freezing and blockage formation of core materials flowing into flow channels such as a pin bundle, inter-wrapper gap and control rod guide tube. This model considers two mechanisms which cause the blockage formation at the front of penetrating molten materials. The first mechanism is the increase of solid particle components in a multi-component flow area and Eq. (5-3) is used to define the multiplication factor. The

second mechanism is the loss of fluidity due to the decrease of specific internal energy in each material component and is considered only for fuel and steel. The viscosity multiplication factor for the fuel component is given by

$$S_{mf} = 1 + C_{PVIS} \frac{\alpha_{MP2} \alpha_{L4}}{\alpha_{MP2} (\alpha_{L1} + \alpha_{L4}) - \alpha_{L4}}, \quad (5-4)$$

and the viscosity multiplication factor for steel component is given by

$$S_{mf} = 1 + C_{PVIS} \frac{\alpha_{MP2} \alpha_{L5}}{\alpha_{MP2} (\alpha_{L2} + \alpha_{L5}) - \alpha_{L5}}, \quad (5-5)$$

where the maximum packing fraction α_{MP2} is an input parameter with the default value 0.9. The second mechanism compensates the deficiency of the first model, where the particle components in the leading edge of the penetrating molten material cannot be stopped if the volume fraction of the particle in a finite-differencing mesh is small. If this second model is not activated (MXFOPT(7)=0), the viscosity multiplication factor S_{mf} is set to unity.

5.2. MXFs between Continuous Fluid and Structure Components

For channel flows, the MXFs between continuous liquid components and structure surface are modeled based on Blasius formula which gives the friction factor for a turbulent flow in a smooth pipe when the Reynolds number of flow is larger than $Re_0 = 3000$,

$$f = \frac{0.0791}{Re^{1/4}}. \quad (5-6)$$

For a laminar flow, in which Reynolds number is less than $Re_0 = 3000$, the Hagen-Poiseuille law is used as a fiction factor such as,

$$f = \frac{16}{Re}. \quad (5-7)$$

Using these formulae, the momentum exchange function in SIMMER-III could be formulated as follows,

$$A_{Lm, s} = \frac{2\alpha_{Lm, s}\mu_L}{\alpha_{Lm}}, \text{ and} \quad (5-8)$$

$$B_{Lm, s} = \frac{1}{2} \alpha_{Lm, s} \rho_{Lm} C_{T1} \left(\frac{4\alpha_{Lm} \rho_{Lm} v_{q(Lm)}}{\alpha_{Lm, s} \mu_L} \right)^{C_{T2}}, \quad (5-9)$$

where the default values of the parameters are: $C_{T1} = 0.0791$ and $C_{T2} = -0.25$.

The viscosity in these equations is simply obtained by multiplying the weighted harmonic mean of the viscosity of existing liquid components with the multiplication factor of particle viscosity model as follows,

$$\mu_L = \left(\sum_{Lm=1,2,3} \alpha_{Lm} / \sum_{Lm=1,2,3} \frac{\alpha_{Lm}}{\mu_{Lm}} \right) \max(S_f, S_{mf}). \quad (5-10)$$

When the flow is regarded as a pool flow, where the effect of structure surface on the flow is small, the MXFs between the continuous fluids and the structure surfaces are simplified as follows,

$$A_{Lm,s} = \frac{2a_{Lm,s}\mu_L}{\alpha_{Lm}}, \text{ and} \quad (5-11)$$

$$B_{Lm,s} = \frac{0.005}{2} a_{Lm,s} \rho_{Lm}. \quad (5-12)$$

5.3. MXFs between Dispersed Fluid and Structure Components

It is assumed that the time scale of the contact between the dispersed fluids and the structure surface is too small for laminar boundary layer to form at the contact interface, only the turbulence term with constant friction factor is used as follows,

$$A_{Lm,s} = 0 \text{ and } B_{Lm,s} = \frac{0.005}{2} a_{Lm,s} \rho_{Lm}. \quad (5-13)$$

Since standard two-phase pressure drop correlations are not applicable in the three-field situations, the momentum exchange functions between continuous fluids and the structure are calculated separately by Reynolds number correlations. Here the effective hydraulic diameters are defined by the respective binary contact areas and the fluid volume fractions.

5.4. Special models in Fluid-Structure MXF

5.4.1. Introduction of Ueda's model

The pressure drop of two-phase flow in a pipe is one of the important phenomena in simulating the event progression in CDA. The general trend of the two-phase pressure drop is represented by Lockhart-Martinelli (L-M) correlation. However, experimental data showed a large discrepancy from this correlation depending on the flow situation, especially in the case of low liquid velocity²³). One cause of this discrepancy is the effect of turbulence enhancement in the liquid phase by the presence of the gas phase. Because L-M correlation is based on the separated flow model, it does not consider the effect of gas-liquid interaction. In order to adopt this mechanism into the pressure drop prediction, some models and semi-empirical correlations were proposed in the literature. After a comparative evaluation of these correlations, a model proposed by Ueda²⁴) is employed in SIMMER-III. A brief description of the model is given in Appendix B.

5.4.2. Particle jamming model

Consider a situation where solid particles flow into a cavity and accumulate from the bottom. The solid particles usually cannot occupy all the space in the cavity and their volume fraction has a certain maximum value. This phenomenon is usually referred to as ‘‘particle jamming’’. In SIMMER-III, this is modeled by preventing the inflow of solid particles into a cell when the volume fraction of solid particles in the cell exceeds a maximum packing fraction by assigning a large value to the MXF at the cell interface.

The concept of this model is to define a function of volume fraction of the particles, which increases exponentially with the increase of the volume fraction of the particles and to add this function to the MXFs

at the cell boundary, which has the incoming flow direction to the jamming cell. The following function is used in SIMMER-III,

$$\varphi = \max \left\{ 1 - \frac{\max[(\alpha_p - A_{pj}B_{pj}), 0]}{A_{pj}(1 - B_{pj})}, 0.1 \right\}^{C_{PJ}} - 1, \quad (5-14)$$

where the default value of each parameter is $A_{pj} = 0.7$, $B_{pj} = 0.95$ and $C_{PJ} = -10.0$. This function remains 0.0 when $\alpha_p \leq A_{pj}B_{pj}$ holds and increases rapidly when α_p exceeds $A_{pj}B_{pj}$. In the implementation in SIMMER-III, the direction of the flow velocity at the cell interface determines the donor cell and the acceptor cell. Equation (5-14) is evaluated using the particle volume fraction in the acceptor cell and the resulting φ is added to the MXF between the particle component and the structure, making this model effective even for the cells without structure component. This model has two options specified MXFOPT(10+n). If MXFOPT(10+n)=0, the volume fractions of all solid particle components are summed to calculate α_p for the evaluation of φ for n-th velocity field. If MXFOPT(10+n)=1, this summation is performed only for the solid particle components belonging to the n-th velocity field.

5.4.3. Particle chunk model

The particle viscosity model treats the frictional force between the solid particle and the structure and the particle jamming model treats the geometric limitation in the sedimentation of solid particles. As the third model to control the motion of solid particles in SIMMER-III, a particle chunk model is implemented to consider the blockage formation of solid particles at the contraction point in a flow channel. This model uses the same algorithm as the SAS4A code and is described in detail in Appendix C. This model is applied only to the fuel chunks component when this fuel chunk model is activated (HMTOPT(69)=1); otherwise the model is applied to both fuel particles and fuel chunks.

6. Averaging of Momentum Exchange Functions

Elemental momentum exchange functions are defined for each energy component in each flow region, such as the bubbly flow region with the first continuous component ($B1$), the bubbly flow region with the second continuous component ($B2$) and the dispersed flow region (D). In order to obtain the overall MXFs between a pair of momentum fields in a finite-differenced cell, these elemental MXFs need to be averaged. This averaging procedure is performed in two steps. First, the elemental MXFs between the energy components are averaged to obtain the MXFs for momentum fields. Second, the MXFs between momentum fields are averaged to obtain the overall MXFs. Since the elemental MXFs can differ by more than an order of magnitude between bubbly and dispersed flow regime regions, this averaging procedure uses a logarithmic interpolation procedure, which is similar to the interpolation of heat-transfer coefficients between different flow regimes.

The first averaging procedure to combine the energy-component-wise elemental MXFs to the MXFs between momentum fields uses the following equations,

$$\alpha_{Lm, Lk, R} = \min(\alpha_{Lm, R}, \alpha_{Lk, R}), \quad (6-1)$$

$$K_{Lm, Lk, R} = A_{Lm, Lk, R} + B_{Lm, Lk, R} |\vec{v}_{q(Lm)} - \vec{v}_{q(Lk)}|, \quad (6-2)$$

$$\xi_{Lm, Lk, R} = \alpha_{Lm, Lk, R} / \sum_{q(Lm)=qm, q(Lk)=qk, Lm \neq Lk} \alpha_{Lm, Lk, R}, \quad (6-3)$$

$$K_{Geom, R} = \exp \left\{ \sum_{q(Lm)=qm, q(Lk)=qk, Lm \neq Lk} \xi_{Lm, Lk, R} \ln \left[\frac{K_{Lm, Lk, R}}{\xi_{Lm, Lk, R}} \right] \right\}, \quad (6-4)$$

$$K_{Arith, R} = \sum_{q(Lm)=qm, q(Lk)=qk, Lm \neq Lk} K_{Lm, Lk, R}, \quad (6-5)$$

$$A_{qm, qk, R} = \frac{K_{Geom, R}}{K_{Arith, R}} \sum_{q(Lm)=qm, q(Lk)=qk, Lm \neq Lk} A_{Lm, Lk, R}, \text{ and} \quad (6-6)$$

$$B_{qm, qk, R} = \frac{K_{Geom, R}}{K_{Arith, R}} \sum_{q(Lm)=qm, q(Lk)=qk, Lm \neq Lk} B_{Lm, Lk, R}, \quad (6-7)$$

where the suffix R denotes the flow regime region area such as $B1$, $B2$ and D .

The averaging procedure of the MXFs between fluid components and structure surfaces are performed using the same algorithm, except that the suffix “ Lm, Lk, R ” in Eqs. (6-2) to (6-7) is replaced by “ Lm, R ” and the summation is performed only for the fluid components satisfying the condition $q(Lm) = qm$.

The second averaging procedure to combine the flow-regime-wise MXFs to the overall MXFs uses the same algorithm as shown in the following equations which describe the algorithm for fluid-fluid MXFs. The

averaging procedure of fluid-structure MXFs can be obtained by simply replacing the suffixes “ qm, qk, R ” in these equations with “ qm, S, R ”.

$$\alpha_{qm, qk, R} = \min(\alpha_{qm, R}, \alpha_{qk, R}), \quad (6-8)$$

$$K_{qm, qk, R} = A_{qm, qk, R} + B_{qm, qk, R} |\vec{v}_{qm} - \vec{v}_{qk}|, \quad (6-9)$$

$$\xi_{qm, qk, R} = \alpha_{qm, qk, R} / \sum_{R=B1, B2, D} \alpha_{qm, qk, R}, \quad (6-10)$$

$$K_{Geom} = \exp \left\{ \sum_{R=B1, B2, D} \xi_{qm, qk, R} \ln \left[\frac{K_{qm, qk, R}}{\xi_{qm, qk, R}} \right] \right\}, \quad (6-11)$$

$$K_{Arith} = \sum_{R=B1, B2, D} K_{qm, qk, R}, \quad (6-12)$$

$$A_{qm, qk} = \frac{K_{Geom}}{K_{Arith}} \sum_{R=B1, B2, D} A_{qm, qk, R}, \text{ and} \quad (6-13)$$

$$B_{qm, qk} = \frac{K_{Geom}}{K_{Arith}} \sum_{R=B1, B2, D} B_{qm, qk, R}. \quad (6-14)$$

Since SIMMER-III employs an Eulerian staggered-mesh finite-differencing scheme, the MXFs must be defined at cell boundary, i.e. at the center of the momentum cell. This is done by interpolating the cell-centered MXF using weighted averaging by mesh cell size. For the fluid-structure MXFs, there is another option to use the MXFs in the upwind cell (MXFOPT(7)=1). This option is recommended to be activated with the new particle viscosity model (MXFOPT(7)=1), since this alleviates the artificial blockage formation by small amounts of solid particle at the leading edge of the penetrating molten material.

7. Verification and Validation

7.1. SIMMER-III Assessment Program

A verification and validation (V&V) program for SIMMER-III has been discussed since the beginning of the code development program. Furthermore so-called “developmental assessment” has been conducted as new models were proposed and developed. A good example is the IFA model development, where a simple test code was first developed and extensively tested for single-cell (zero-th dimension) problems before the models were actually programmed in SIMMER-III. The fluid convection algorithm and boundary conditions were also thoroughly tested in an early adiabatic version of the code without models for heat and mass transfer.

The SIMMER-III V&V program, called the “code assessment program”, was conducted in two steps, Phase 1 and Phase 2.^{25), 26)} The Phase 1 assessment is intended to verify individual fluid-dynamics models of the code, whilst Phase 2 is intended to provide comprehensive validation for integral and inter-related accident phenomena, such as transient fuel motion during the transition phase and high-pressure CDA bubble expansion in the post-disassembly expansion phase. Direct application of the code to complex accident phenomena involves many inter-related processes to be solved simultaneously and is not always productive. Thus, the present step-by-step approach is advantageous, since in Phase 1 the coding is largely debugged and verified, and each major model is validated separately.

7.2. Results of Phase 1 Assessment

In Phase 1 assessment, SIMMER-III is applied to a variety of fluid-dynamics test problems with the objective of validating individual models separately as far as possible. The test problems are therefore categorized as follows: fluid convection algorithm, interfacial areas and momentum exchange functions, heat transfer coefficients, melting and freezing, and vaporization and condensation. In the Phase 1 report, the results of assessment on the MXF modeling were summarized as follows.

The MXFs are based on quasi-steady state engineering correlations for well-defined topologies. They are modeled separately for each velocity field and for each flow regime. An assessment of MXFs in pool flow is obtained from the zero-th order calculations of pool flow and the bubble column problem. The MXFs in the bubbly and dispersed flow regimes are found to be satisfactory, and the interpolation procedure is believed to provide a sufficiently smooth and valid means of treating the transition flow regime. However, the need to model the drag between vapor-continuous and liquid-continuous regions of transition flow was also identified. The pressure drop in pipe flow was underestimated by the original model due to the lack of a proper treatment of turbulent enhancement in the liquid phase by the relative motion of vapor. A later improvement to the liquid-structure MXF to account for this effect enabled SIMMER-III to reproduce well the pressure drop characteristics in pipe flow.

The MXFs between gas and liquid in annular dispersed flow need to be improved to compensate for the large difference between droplet and film velocities. It was also found that SIMMER-III underestimates the vapor-liquid film momentum coupling in pure annular flow. This is probably because the formation of ripples

on the surface of liquid films enhances the momentum coupling, and this effect is not currently modeled by the code.

Not all of the test problems studied in Phase 1 were satisfactory; problem areas were identified and the areas for model improvement were recommended. Model improvements were continued and some of the test problems were re-calculated in Phase 2.

7.3. Results of Phase 2 Assessment

In Phase 2 assessment, SIMMER-III is applied to test problems relevant to key accident phenomena in LMFR such as: boiling pool dynamics, fuel relocation and freezing, material expansion, fuel-coolant interactions (FCIs), structure disintegration and disrupted core neutronics. In the synthesis compiled in the Phase 2 report, the results on the assessment of the flow regime and momentum exchange models are evaluated and summarized as follows.

The multiple flow regime treatment in SIMMER-III is based on simple flow regime maps to describe both the pool and channel flows as a function of vapor volume fraction. This simple treatment can still adequately represent a multi-component system. The Phase 1 and Phase 2 assessment programs have demonstrated that the flow regime model is mostly appropriate for describing various multi-flow topology over whole range of void fractions with smooth transition between flow regimes. The models for IFA, MXF and HTC are designed to be consistent with the flow-regime modeling framework. The model improvement for the bubbly flow regime has been made to consider cap-shape bubbles observed in a higher vapor velocity and thereby improving the vapor-liquid momentum coupling.

Although the MXFs, which are basically based on engineering correlations for the individual flow regimes, are mostly validated, there remain fundamental difficulties in describing the interpolated flow regime in the intermediate void fraction range. This is partly due to the lack of detailed experimental evidence on multi-phase flow topology sufficient to develop a more mechanistic model. There is also a difficulty in representing an annular-dispersed flow where the SIMMER-III framework cannot distinguish droplets from liquid film (of a same liquid material) on the structure surface.

In some of the test problems studied in Phase 1, where various small-scale single- and two-phase flow experiments were analyzed, the neglect of radial inter-cell momentum coupling in early versions of SIMMER-III was criticized and considered as one of the reasons for the poor re-reproducibility. Later during the Phase 2 study, a viscous drag term (momentum diffusion model) was developed for SIMMER-III and applied to some of the test problems, showing obvious improvements especially in simulating laminar or low velocity flow experiments. It is noted, however, that in the multi-component, multi-velocity fluid dynamics system, with different flow regimes, the implementation of the model requires a complex procedure to judge whether the momentum diffusion is to be treated. A turbulence model has long been desired for SIMMER-III, and indeed a simple model applicable only to specific situations was also attempted in Phase 2. However, a more fundamental study is needed.

The flows containing particles need to be addressed further in the future and possible model refinement. The main interest is its relevance to fuel freezing and relocation. The fundamental difficulty of distinguishing

between frozen particles and broken-up pin fuel chunks may have to be addressed to some extent. This difficulty has been later improved by adding a “fuel chunks” component that has different density and energy from fuel particles.

8. Conclusion

In this study, a closed set of formulations of the momentum exchange functions (MXFs) was developed for SIMMER-III and SIMMER-IV. The MXF model consistently covers the multiphase flow regimes which are commonly used in the interfacial area and the heat transfer coefficient models. These constitutive models are applicable to various multi-component multi-phase flow situations over a whole range of void fraction with smooth transition. The fluid-fluid MXF model was formulated based on the ordinary correlations for two-phase flows. The fluid-structure MXF in multi-phase multi-component flow was developed by analogy to the separated flow model for two-phase flows, whilst the interactions among the components are considered by fluid-fluid MXFs. The particle viscosity model, particle jamming model and particle chunk model were developed to adequately simulate the blockage formation in molten material penetration into structure channels.

These frameworks made SIMMER-III/SIMMER-IV flexible and applicable to a wide range of complex multi-phase flow in a degraded core of LMFR.

Acknowledgment

The authors are indebted to W. R. Bohl of the Los Alamos National Laboratory for his significant contribution to forming the basis of SIMMER-III. The authors would like to acknowledge K. Morita (presently with Kyushu University) and X. Cao (presently with Shanghai Jiao Tong University) for their effort in development of special models. Collaborating efforts by the staff members of JAEA (the former PNC or JNC) are greatly acknowledged, including N. Shirakawa, K. Kamiyama and H. Yamano. Our special thanks are due to M. Sugaya and F. Inoue in programming and debugging, and computational assistance.

References

- 1) Kondo, S. et al., SIMMER-III and SIMMER-IV: Computer Codes for LMFR Core Disruptive Accident Analysis, JAEA-Research 2024-008, 2024, 235p.
- 2) Morita, K. et al., SIMMER-III Analytic Equation-of-State Model, JNC TN9400 2000-005, 1999, 57p.
- 3) Morita, K. et al., SIMMER-III Analytic Thermophysical Property Model, JNC TN9400 2000-004, 1999, 38p.
- 4) Morita, K. et al., SIMMER-III/IV Heat- and Mass-Transfer Model - Model and Method Description -, JNC TN9400 2003-047, 2003, 109p.
- 5) Kamiyama, K. et al., SIMMER-III Structure Model - Model and Method Description -, JNC TN9400 2004-043, 2004, 83p.
- 6) Brear, D.J. et al., Heat-Transfer Coefficients Model for SIMMER-III and SIMMER-IV, JAEA-Research 2024-009, 2024, 134p.
- 7) Tobita, Y. et al., Multi-Phase Flow Topology and Interfacial Area Model for SIMMER-III and SIMMER-IV, JAEA-Research 2024-010, 2024, 77p.
- 8) Bohl, W.R., Luck, L.B., SIMMER-II: A Computer Program for LMFBR Disrupted Core Analysis, LA-11415-MS, Los Alamos National Laboratory, 1990.
- 9) Bohl, W.R. et al., AFDM: An Advanced Fluid Dynamics Model, LA-11692-MS, Los Alamos National Laboratory, 1990.
- 10) Wilhelm, D. et al., AFDM: An Advanced Fluid Dynamics Model, Volume II: Topologies, Flow Regimes and Interfacial Areas, LA-11692-MS, Vol. II, Los Alamos National Laboratory, 1990.
- 11) Ishii, M., Zuber, N. et al., Drag Coefficient and Relative Velocity in Bubbly, Droplet or Particulate Flows, AIChE J., vol. 25, 1979, pp.843-855.
- 12) Cao, X., Tobita, Y., Study on Drag Coefficient for the Particle/Droplet with Vapor Film, JNC TN9400 2001-055, 2000, 40p.
- 13) Cao, X., Tobita, Y., Simulation of Premixing Experiment QUEOS by SIMMER-III, JNC TN9400 2000-100, 2000, 45p.
- 14) Mishima, K. et al., Visualization and Measurement of Gas-Liquid Two-Phase Flow with Large Density Difference Using Thermal Neutrons as Microscopic Probes, Nuclear Instruments and Methods in Physics Research, 424, 1999, pp.229-234.
- 15) Kataoka, I., Ishii, M., Drift Flux Model for Large Diameter Pipe and New Correlation for Pool Void Fraction, Int. J. Heat Mass Transfer, vol.30, no.9, 1987, pp.1927-1939.
- 16) Hibiki, T., Study on Flow Characteristics in Gas-Molten Metal Mixture Pool, Nuclear Engineering and Design, 196, 2000, pp.233-245.
- 17) Suzuki, T., Tobita, Y. et al., Analysis of gas-liquid metal two-phase flows using a reactor safety analysis code SIMMER-III, Nuclear Engineering and Design, 220(3), 2003, pp.207-223.

- 18) Ishii, M., Chawla, T.C., Local Drag Laws in Dispersed Two-Phase Flow, Argonne National Laboratory report, ANL-79-105, 1979.
- 19) Grace, J.R., Shapes and Velocities of Bubbles Rising in Infinite Liquids, *Trans. Inst. Chem. Engrs.*, 51, 1973, pp.116-120.
- 20) Grace, J.R., Shapes and Velocities of Single Drops and Bubbles, *Trans. Inst. Chem. Engrs.*, 54, 1976, pp.167-173.
- 21) Clift, R., Grace, J.R., Weber, M.E., *Bubbles, Drops and Particles*, Academic Press, New York, 1978, pp.22-28.
- 22) Bohl, W.R., *AFDM: An Advanced Fluid Dynamics Model, Volume V: The Convective Transport Algorithm*, LA-11692-MS, Vol. V, Los Alamos National Laboratory, 1990.
- 23) Inoue, A., Aoki, S., Basic study on the pressure drop in two-phase flow in a pipe, *Nihon-kikai-gakkai ronbunshu* (in Japanese), vol.32, no.238, 1966, pp.940-947.
- 24) Ueda, T., On the upward flow of gas-liquid mixture in a pipe, *Nihon-kikai-gakkai ronbunshu* (in Japanese), vol.33, no.248, 1967, pp.601-625.
- 25) Kondo, S. et al., Phase 1 Code Assessment of SIMMER-III, A Computer Program for LMFR Core Disruptive Accident Analysis, JAEA-Research 2019-009, 2019, 382p.
- 26) Kondo, S. et al., Phase 2 Code Assessment of SIMMER-III, A Computer Program for LMFR Core Disruptive Accident Analysis, JNC TN9400 2000-105, 2000, 777p.
- 27) Einstein, A., Eine neue Bestimmung der Molekül-dimensionen, *Annalen der Physik*, 1906.
- 28) Batchelor, G.K., The effect of Brownian motion on the bulk stress in a suspension of spherical particles, *J. Fluid Mech.*, 83, 1, 1977, pp.97-117.
- 29) Thomas, D.G., Transport characteristics of suspension: VIII. A note on the viscosity of Newtonian suspensions of uniform spherical particles, *J. Colloid Sci.*, 20, 1965, pp.267-277.
- 30) Mooney, M., The viscosity of a concentrated suspension of spherical particles, *J. Colloid Sci.*, 6, 1950, pp.162-170.
- 31) Frankel, N.A., Acrivos, A., On the viscosity of a concentrated suspension of solid spheres, *Chem. Eng. Sci.*, 22, 1967, pp.847-853.
- 32) Krieger, I.M., Rheology of monodisperse latices, *Adv. Colloid and Interface Sci.*, 3, 1972, pp.111-136.
- 33) Langmaid, R.N., Rose, H.E., Archformation in a Non-cohesive Granular Material, *Journal of the Institute of Fuel*, 166, 1957.

Table 1. SIMMER-III/SIMMER-IV fluid-dynamics structure-field components.

Density components (MCSR)		Energy components (MCSRE)	
S-III/S-IV*		S-III/S-IV*	
s1	Fertile pin fuel surface node	S1	Pin fuel surface node
s2	Fissile pin fuel surface node		
s3	Left fertile crust fuel	S2	Left crust fuel
s4	Left fissile crust fuel		
s5	Right fertile crust fuel	S3	Right crust fuel
s6	Right fissile crust fuel		
--/s7	Front fertile crust fuel*	--/S4	Front crust fuel*
--/s8	Front fissile crust fuel*		
--/s9	Back fertile crust fuel*	--/S5	Back crust fuel*
--/s10	Back fissile crust fuel*		
s7/s11	Cladding	S4/S6	Cladding
s8/s12	Left can wall surface node	S5/S7	Left can wall Surface node
s9/s13	Left can wall interior node	S6/S8	Left can wall Interior node
s10/s14	Right can wall surface node	S7/S9	Right can wall Surface node
s11/s15	Right can wall interior node	S8/S10	Right can wall Interior node
--/s16	Front can wall surface node*	--/S11	Front can wall surface node*
--/s17	Front can wall interior node*	--/S12	Front can wall interior node*
--/s18	Back can wall surface node*	--/S13	Back can wall surface node*
--/s19	Back can wall interior node*	--/S14	Back can wall interior node*
s12/s20	Control	S9/S15	Control

* The front and back can walls are modeled in a three-dimensional code, SIMMER-IV, in addition to the left and right can walls.

Table 2. SIMMER-III/SIMMER-IV fluid-dynamics liquid-field components.

Density components “ <i>m</i> ” (MCLR)		Energy components “ <i>M</i> ” (MCLRE)		Velocity fields “ <i>q</i> ”	
				default	recommended
<i>l1</i>	Liquid fertile fuel	<i>L1</i>	Liquid fuel	<i>q1</i>	<i>q1</i>
<i>l2</i>	Liquid fissile fuel			<i>q1</i>	<i>q1</i>
<i>l3</i>	Liquid steel	<i>L2</i>	Liquid steel	<i>q2</i>	<i>q2</i>
<i>l4</i>	Liquid sodium	<i>L3</i>	Liquid sodium	<i>q2</i>	<i>q3</i>
<i>l5</i>	Fertile fuel particles	<i>L4</i>	Fuel particles	<i>q1</i>	<i>q1</i>
<i>l6</i>	Fissile fuel particles			<i>q1</i>	<i>q1</i>
<i>l7</i>	Steel particles	<i>L5</i>	Steel particles	<i>q1</i>	<i>q2</i>
<i>l8</i>	Control particles	<i>L6</i>	Control particles	<i>q2</i>	<i>q4</i>
<i>l9</i>	Fertile fuel chunks	<i>L7</i>	Fuel chunks	<i>q2</i>	<i>q5</i>
<i>l10</i>	Fissile fuel chunks			<i>q2</i>	<i>q5</i>
<i>l11</i>	Fission gas in liquid fuel			<i>q1</i>	<i>q1</i>
<i>l12</i>	Fission gas in fuel particles			<i>q1</i>	<i>q1</i>
<i>l13</i>	Fission gas in fuel chunks			<i>q2</i>	<i>q5</i>

Table 3. SIMMER-III/SIMMER-IV fluid-dynamics vapor-field components.

(MCGR)		(material component) *		Velocity fields “ <i>q</i> ”	
				default	recommended
<i>g1</i>	Fertile fuel vapor	<i>G1</i>	Fuel vapor	<i>q3</i>	<i>q6</i>
<i>g2</i>	Fissile fuel vapor			<i>q3</i>	<i>q6</i>
<i>g3</i>	Steel vapor	<i>G2</i>	Steel vapor	<i>q3</i>	<i>q6</i>
<i>g4</i>	Sodium vapor	<i>G3</i>	Sodium vapor	<i>q3</i>	<i>q6</i>
<i>g5</i>	Fission gas	<i>G4</i>	Fission gas	<i>q3</i>	<i>q6</i>

* All vapor components, behaving as a vapor mixture and having the same temperature, are treated as a single energy component “*G*” and assigned to the same velocity field.

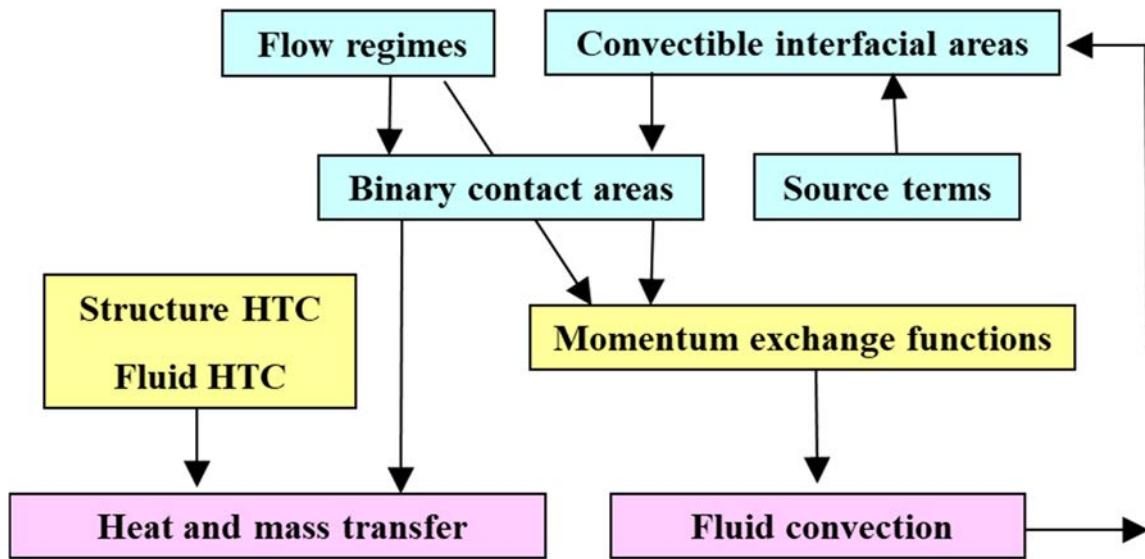


Fig. 1. Roles of the MXF model in SIMMER-III/SIMMER-IV.

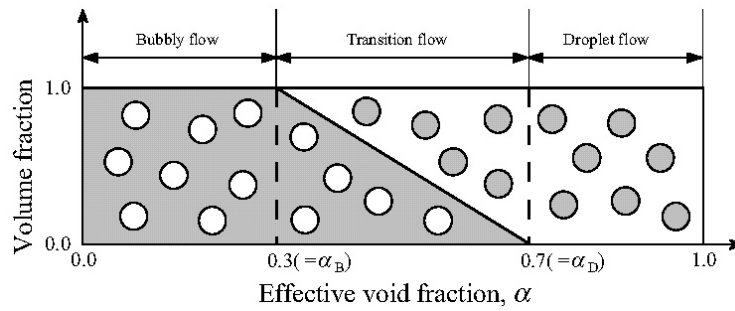


Fig. 2. Pool flow regime map in SIMMER-III.

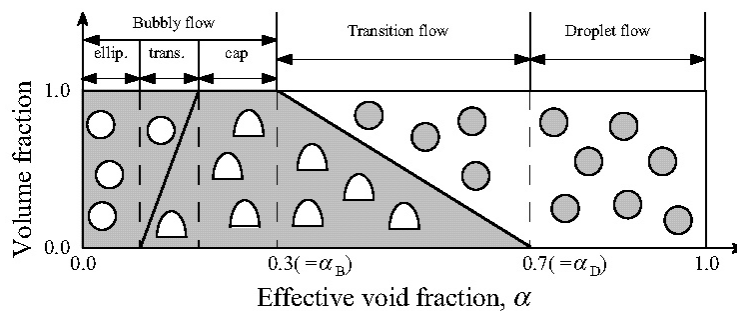


Fig. 3. Pool flow regime map with cap bubble flow regime in SIMMER-III.

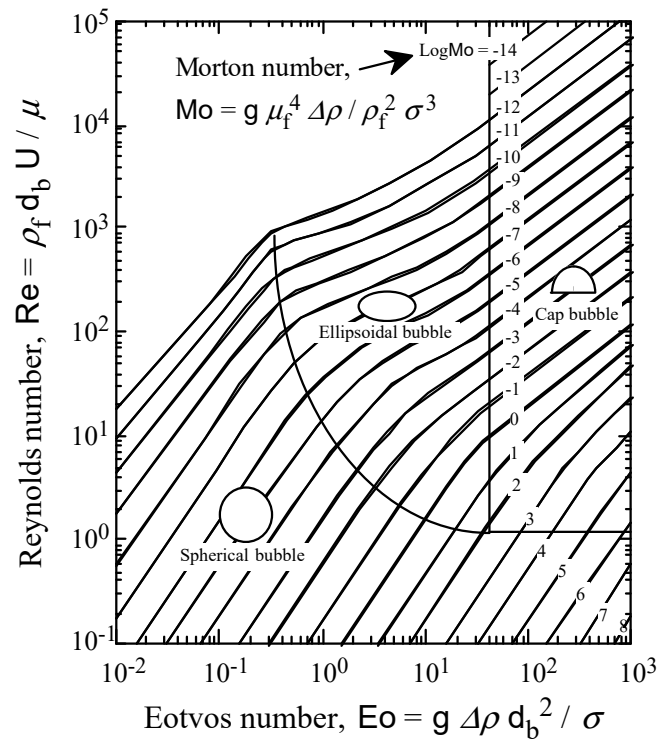


Fig. 4. Bubble shape map.

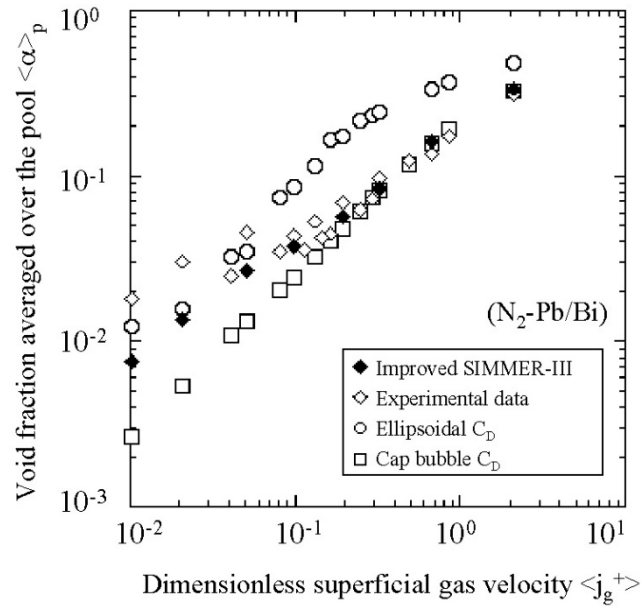


Fig. 5. Results of code improvement for cap bubble flow regime.

Appendix A Formulation of Particle Viscosity

1. Correlations for Effective Particle Viscosity

It is well known that the apparent viscosity of a solid particle suspension in a liquid is greater than that of the liquid itself. Consideration of this apparent viscosity increase is important when simulating the penetration of molten material into the flow path of a cold structure and the formation of blockage. Since the increase of effective or apparent viscosity is caused by the interaction between the particles and the interaction of the liquid component with the solid particles, it is reasonable to relate the effective viscosity to the volume fraction of the particle component. Einstein²⁷⁾ deduced the following correlation for infinite dilute latex:

$$\eta_r = 1 + 2.5\alpha_p, \quad (\text{A-1})$$

where η_r is the ratio of the effective viscosity of the mixture to the viscosity of liquid, and α_p is the volume fraction of solid particles. Other correlations have been proposed by many researchers up to now. Some of them are the simple extensions of Einstein's correlation by adding higher order terms and thus being applicable to smaller particle volume fractions:

$$\eta_r = 1 + 2.5\alpha_p + C\alpha_p^2 + O(\alpha_p^3). \quad (\text{A-2})$$

The coefficient C is given as 6.2 by Batchelor²⁸⁾ and 10.05 by Thomas²⁹⁾. Other correlations introduced the inverse of $1 - \alpha_p/\alpha_{max}$ to simulate the steep increase of the effective viscosity near the closed packing fraction of solid particle α_{max} . For example, Mooney³⁰⁾ proposed the following formulation:

$$\eta_r = \exp\left(\frac{2.5\alpha_p}{1 - \alpha_p/\alpha_{max}}\right), \quad (\text{A-3})$$

where the coefficient 2.5 was determined by the requirement that the formulation should reduce to Einstein's correlation at the infinite dilute suspension ($\alpha_p \rightarrow 0$). If we take the first term of the series expansion of Mooney's correlation, it will give:

$$\eta_r = 1 + \frac{2.5\alpha_p}{1 - \alpha_p/\alpha_{max}}. \quad (\text{A-4})$$

For the SIMMER-II and AFDM code, the following expression is used.

$$\eta_r = 1 - \alpha_p + \frac{C\alpha_p}{1 - \alpha_p/\alpha_{max}}, \quad (\text{A-5})$$

where the coefficient C is an adjusting parameter. The derivative of this correlation becomes $C - 1$ at the infinitely dilute suspension, which also reduces to Einstein's correlation with $C = 3.5$.

As a correlation of the effective viscosity for the volume fraction of solid particles near the closed packing fraction, Frankel and Acrivos³¹⁾ proposed the following correlation by focusing on the energy dissipation in the small gap between particles:

$$\eta_r = \frac{9}{8} \frac{\alpha_{max}^{1/3} \alpha_p^{1/3}}{\alpha_{max}^{1/3} - \alpha_p^{1/3}}. \quad (A-6)$$

2. Experimental Data

Thomas²⁹⁾ made an extensive survey of experimental data and organized them by considering colloid-chemical forces and additional energy dissipation mechanism by inertial effects due to the restoration of particle rotation after collision. The experimental data reviewed covered the data measured with both rotational and capillary viscometers and represented a range of particle diameters from 0.099 to 435 microns, including the particle materials of polystyrene, rubber latex, glass, and methyl methacrylate. Krieger³²⁾ also made the same correction to his experimental data with polystyrene particles ranging in diameter from 0.2 to 1.1 microns.

3. Comparison of the Correlations with Experimental Data

The correlations (A-2) to (A-6) are compared with the experimental data in Fig. A.1. In this comparison, the closed packing fraction is fixed to 0.62, following the suggestion by Ishii¹¹⁾ for solid particles in his similarity hypothesis law, which is the basis of the drag coefficient model in SIMMER-III and SIMMER-IV. The least-squares fit of the correlation (A-5) to the experimental data gives $C=3.17$, but 3.5 is used in this comparison, to account for the reduction to Einstein's correlation (A-1) at the infinite dilute suspension. Both Eqs. (A-4) and (A-5) give reasonable fits to the experimental data, and Eq. (A-5) gives slightly better result. Mooney's correlation overestimates the experimental data with closed packing fraction of 0.62. However, the least-squares fit of the closed packing fraction in Mooney's correlation gives 0.92 and Mooney's correlation results in the best fit to the experimental data with this value among the correlations. Both Thomas' and Frankel's correlations give reasonable agreement for lower volume fraction region and higher volume fraction region, respectively.

4. Consideration

From the comparison of the existing correlations and experimental data for the effective viscosity ratio of solid particle suspension in liquid, Eqs. (A-4) and (A-5) give fairly good agreement with the experimental data, and Eq. (A-5) is slightly closer to the experimental data than the other correlations. Mooney's correlation (A-3) also gives good results, if 0.92 is used as the closed packing fraction. This value is higher than the theoretical maximum value of packing fraction of solid spheres, 0.74. Based on these results, Eq. (A-5), is used in SIMMER-III and IV, with the default parameter $C = 3.5$.

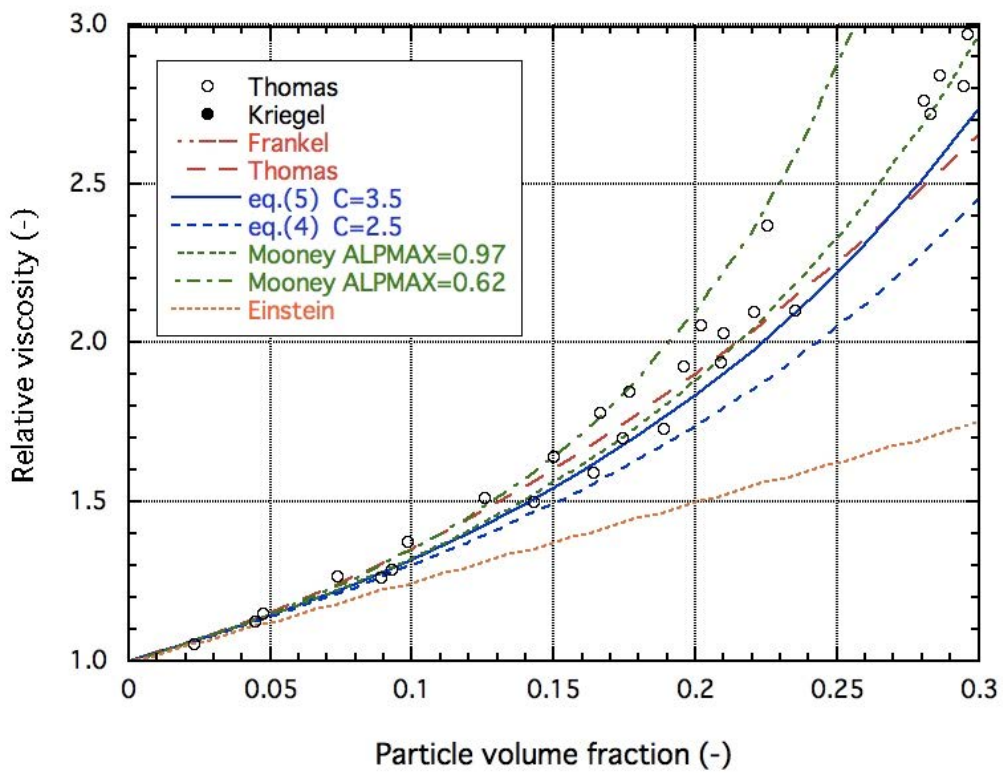
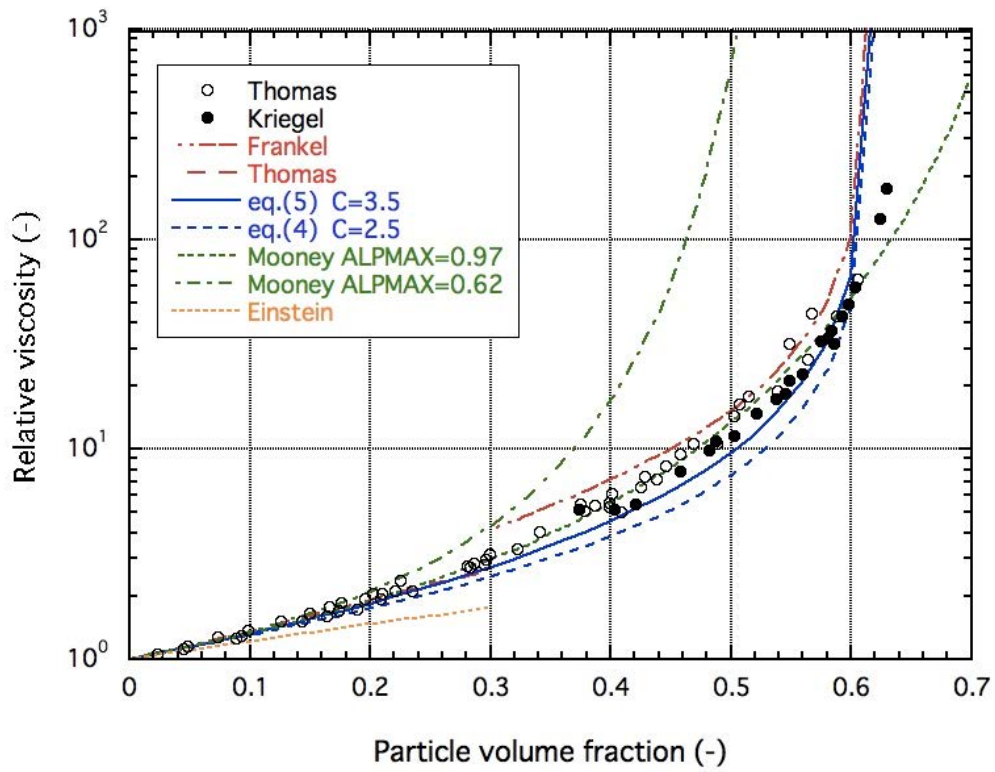


Fig. A.1 Comparison of the correlations and experimental data of effective viscosity ratio of solid particle suspension in liquid

Appendix B Ueda's Model

The relationship between the pressure drop and the shear stress at the wall is given by

$$\frac{\Delta P}{\Delta L} = \frac{2}{r} \tau,$$

since

$$\pi r^2 \Delta P = 2\pi r \tau_0 \Delta L.$$

The pressure balance in the vapor core in annular flow yields

$$\frac{\Delta P}{\Delta L} = \rho_g g + \frac{2}{r_i} \tau_i. \quad (\text{B-1})$$

If we define τ_0 as the shear force at wall surface, the following equations hold:

$$\tau_0 = \frac{r_0}{2} \left(\frac{\Delta P}{\Delta L} \right)_{TP},$$

$$\frac{\Delta P}{\Delta L} = \alpha \rho_g g + (1 - \alpha) \rho_\ell g + \left(\frac{\Delta P}{\Delta L} \right)_{TP},$$

and

$$\frac{\Delta P}{\Delta L} = \left(\frac{r_i}{r_0} \right)^2 \rho_g g + \left[1 - \left(\frac{r_i}{r_0} \right)^2 \right] \rho_\ell g + \frac{2}{r_0} \tau_0. \quad (\text{B-2})$$

Let τ the shear stress at arbitrary location, the force balance in the liquid film,

$$\frac{\Delta P}{\Delta L} = \left(\frac{r_i}{r} \right)^2 \rho_g g + \left[1 - \left(\frac{r_i}{r} \right)^2 \right] \rho_\ell g + \frac{2}{r} \tau,$$

results in

$$\tau = \frac{r}{r_0} \tau_0 + \frac{r}{2} (\rho_\ell - \rho_g) g \left[\left(\frac{r_i}{r} \right)^2 - \left(\frac{r_i}{r_0} \right)^2 \right] = \tau_0 + \varphi y + \frac{\Delta \rho g \alpha}{2} \left(\frac{r_0^2}{r} - 2r_0 + r \right). \quad (\text{B-3})$$

The definition of the shear stress is expressed as

$$\tau = \rho_\ell \nu_\ell \frac{du}{dr}, \quad (\text{B-4})$$

where ν_ℓ is the kinematic viscosity in the laminar layer. The integration of Eq. (B-4) from the wall surface ($y = 0$, $r = r_0$) to the boundary of laminar layer ($r_\delta \leq r \leq r_0$) gives the velocity at the laminar boundary.

$$u_\delta = \frac{1}{\rho_\ell \nu_\ell} \left[\tau_0 \delta + \frac{\varphi}{2} \delta^2 - \frac{\Delta \rho g \alpha}{2} \left(r_0^2 \log \frac{r_0 - \delta}{r_0} + r_0 \delta + \frac{1}{2} \delta^2 \right) \right], \quad (\text{B-5})$$

where

$$\varphi = \Delta\rho g\alpha - \frac{\tau_0}{r_0}.$$

Here we start from the single-phase flow. The wall shear stress is given by

$$\tau_0 = \frac{1}{2}C_D\rho_\ell u_m^2, \quad (\text{B-6})$$

where u_m is the average velocity of liquids. In the single-phase flow, the void fraction is zero ($\alpha = 0$) and Eq. (B-5) becomes

$$u_\delta = \frac{1}{\rho_\ell \nu_\ell} \left[\tau_0 \delta - \frac{\tau_0}{2r_0} \delta^2 \right]. \quad (\text{B-7})$$

Neglecting the second term and substituting Eq. (B-6), we get

$$u_\delta = \frac{\delta C_D u_m^2}{2\nu_\ell}. \quad (\text{B-8})$$

In the developed turbulent flow in single component flow, the thickness of the laminar boundary layer is given by the following non-dimensional length,

$$\delta^+ = \sqrt{\frac{\tau_0 \delta}{\rho v}} = K. \quad (\text{B-9})$$

The non-dimensional velocity at this thickness is defined as

$$u_\delta^+ = u_\delta / \sqrt{\frac{\tau_0}{\rho}}, \quad (\text{B-10})$$

then $u_\delta^+ = \delta^+$.

$$u_\delta^+ \delta^+ = \frac{u_\delta \delta}{\nu} = K^2. \quad (\text{B-11})$$

The generalized flow distribution gives $K = 5$, the assumption of two regimes gives $K = 12$. The flow situation in two-phase flow will be different from that in single phase flow, the value of K should be between 5 and 12, and currently $K = 7$ is assumed. Then, this equation becomes as follows:

$$\delta = 50 \frac{\nu_\ell}{u_\delta}. \quad (\text{B-12})$$

Substituting Eq. (B-12) into Eq. (B-8), the velocity at the laminar boundary layer is given as the function of the mean velocity u_m ,

$$u_\delta = \sqrt{25C_D}. \quad (\text{B-13})$$

In two-phase flow, the flow condition is different from single phase flow, and equation does not hold with its original form. However, the introduction of additional correction term is assumed to give the appropriate effective mean velocity for two-phase flow. In an upward annular flow, the gas velocity is greater

than the liquid velocity and this velocity difference will enhance the turbulence in the liquid film and hence increases. This effect is expressed by the term,

$$\Delta u_{\ell 1} = C_1 Re_s^{C_2} u_s, \quad (\text{B-14})$$

where u_s is the slip velocity, $Re_s = u_s 2y_i / \nu_\ell$, and y_i is the liquid film thickness.

The velocity increase in the turbulence layer should be greater in two-phase flow than in single-phase flow. This mechanism reduces the effective mean velocity. Assuming that the eddy diffusivity is proportional to the distance from the wall and the characteristic velocity u_{ed} which corresponds to the intensity of the turbulence, this effect is expressed by

$$\Delta u_{\ell 2} = C_3 Fr_{ed} u_{ed}, \quad (\text{B-15})$$

where

$$Fr_{ed} = \frac{g\alpha 2y_i}{u_s^2}, \text{ and}$$

$$u_{ed} = j_g + j_\ell.$$

Eventually, the effective mean velocity is given as follow,

$$u_m^* = u_\ell + \Delta u_{\ell 1} - \Delta u_{\ell 2}. \quad (\text{B-16})$$

The experimental data gave the relation between u_m^* and u_δ as

$$u_\delta = \frac{1.10}{Re_m^{1/8}} u_m^*. \quad (\text{B-17})$$

In the case of bubbly flow, the relative motion of bubbles generates turbulence in liquid and then increases u_δ . This effect is expressed by the following correction term.

$$\Delta u_{\ell 3} = C_4 Fr_s^{C_5} u_s^{C_6}, \quad (\text{B-18})$$

where

$$Fr_s = \frac{g\alpha 2y_i}{u_s^2}, \text{ and}$$

$$u_{ed} = j_g + j_\ell.$$

At the limit of $\alpha \rightarrow 0$, the velocity at the laminar boundary layer should reduce to Eq. (B-13). Therefore, the following equation is used for bubbly flow,

$$u_\delta = \sqrt{25 C_D} u_m^*. \quad (\text{B-19})$$

Substituting Eq. (B-12) into Eq. (B-5) and rearranging, we get

$$\tau_{TP} = \frac{\left[\frac{\rho_\ell u_\delta^2}{50} - \frac{50v_\ell}{2u_\delta} \rho_\ell g \alpha \right]}{\left(1 - \frac{50v_\ell}{D_h u_\delta} \right)}. \quad (\text{B-20})$$

The ratio of τ_{TP} to τ_0 gives the pressure drop multiplication factor R in two-phase flow.

SIMMER-III explicitly represents the bubbly and annular flow regimes, while the intermediate regime (slug flow regime) is modeled by a transition flow where a mesh cell is treated as a combination of a bubbly and annular regions. The fraction of the bubble flow region that occupies the structure surface is modeled as the fraction of the contact area of the liquid slug F_{slug} that is in contact with the structure surface. The multipliers in the bubbly flow region and annular flow region are then averaged logarithmically to obtain the overall multiplier as follows.

$$R = R_{bubbly}^{F_{slug}} R_{annular}^{1-F_{slug}}. \quad (\text{B-21})$$

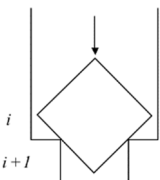
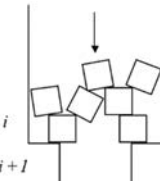
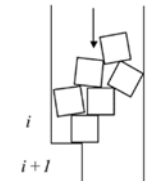
Finally, the coefficients in Eqs. (B-14), (B-15) and (B-18) are determined through a trial-and-error procedure to obtain best agreement with the experimental data as:

$$\begin{aligned} C_1 &= 0.75 \\ C_2 &= -0.25 \\ C_3 &= -12.0 \\ C_4 &= 2.3 \\ C_5 &= 0.3 \\ C_6 &= 1.8 \end{aligned} \quad (\text{B-22})$$

Appendix C Particle Chunk Model

When solid particles flow in a channel with contraction, the particles may jam depending on the size of particles and diameter of channel. There are mainly two mechanisms for the particles to jam, the jamming by large chunk and the jamming by bridge formation. These mechanisms are modeled in the SAS4A code based on the experimental study by Langmaid.³³⁾ The criteria for jamming are summarized in Table C-1. The same criteria are also implemented in SIMMER-III as a whole.

Table C-1. Framework of jamming of particle chunk.

Mode	Illustration	Criteria for jamming
a big chunk		$d_{P,i} > 0.71D_{ch,i+1}$ In pin region, $D_{ch,i+1} = 0.7D_{h,i+1}$. In disrupted region, $D_{ch,i+1} = D_{h,i+1}$
contraction ($\alpha_{P,i} > 0.05$)		If $D_{ch,i+1} < D_{ch,i} - d_{P,i}$, pin region, $d_{P,i} \geq 0.17D_{h,i+1}$ disrupted region, $d_{P,i} \geq 0.24D_{h,i+1}$
		If $D_{ch,i} - d_{P,i} \leq D_{ch,i+1} < D_{ch,i} - 0.5d_{P,i}$, pin region, $d_{P,i} \geq 0.35D_{h,i+1}$ disrupted region, $d_{P,i} \geq 0.50D_{h,i+1}$

This is a blank page.

